Theory and preliminary experimental verification of the directional difference of overland flow resistance in distributed hydrological models

Shengtang Zhang, Yuanchen Liu, Jingzhou Zhang, Ying Liu and Zhikai Wang

ABSTRACT

Overland flow is influenced by the spatial variability of the watershed surface and the distribution of vegetation in the process of confluence. Thus, Manning's roughness coefficient, in different directions on the slope, has different values. This causes different effects on the resistance to flow in the downstream direction of each grid cell, affecting the flow distribution among the grid cells of a distributed hydrological model. To show that the spatial variation of the overland vegetation had the effect of directional difference resistance to the overland flow, this study used an indoor fixed-bed test. We used a cylinder to simulate the stems of the vegetation used in the study. We modeled the relationship between Manning's roughness coefficient and flow depth and studied this relationship for three types of vegetation distributed at three different slopes of 0.0%, 0.5%, and 1.0%. The slopes were based on three angles of 30°, 45°, and 90° between the vegetation rows and flow. The results showed that the resistance of overland flow had directional differences caused by the spatial variability of the vegetation distribution. At the same slope and flow depth, Manning's roughness coefficient decreased as the angle between flow and vegetation rows increased. At the same slope, the angle between flow and vegetation rows and Manning's roughness coefficient increased as flow depth increased. The slope did not affect the law of Manning's roughness coefficient with changes in the angle between flow and vegetation rows.

Key words | directional difference, distributed hydrological model, flow confluence, flow resistance, Manning's roughness coefficient

Shengtang Zhang (corresponding author)
Yuanchen Liu
Jingzhou Zhang
Ying Liu
Zhikai Wang
College of Earth Science and Engineering,
Shandong University of Science and Technology,
Qingdao 266590,
China
E-mail: *zst0077@163.com*

INTRODUCTION

A distributed hydrological model is a powerful tool that can be used conveniently to study the effects of underlying surface changes on hydrological cycle processes. Distributed hydrological models used in the simulation of slope convergence, however, still have trouble determining the flow direction of the slope in the grid cell and the flow distribution algorithm (Shen *et al.* 1995; Li & Li 2000). In the current distributed hydrological model, two main algorithms are used to calculate overland flow direction and flow distribution, which are the single-flow direction and multi-flow direction algorithm.

The D8 algorithm proposed by O'Callaghan & Mark (1984) is the classical single-flow direction algorithm, which considers that the runoff generated by the cell will flow to the lowest cell of eight neighboring cells as shown in Figure 1. The computational complexity of the algorithm is relatively simple, although the data processing efficiency of the grid's discrete element method (DEM) is

doi: 10.2166/ws.2018.040

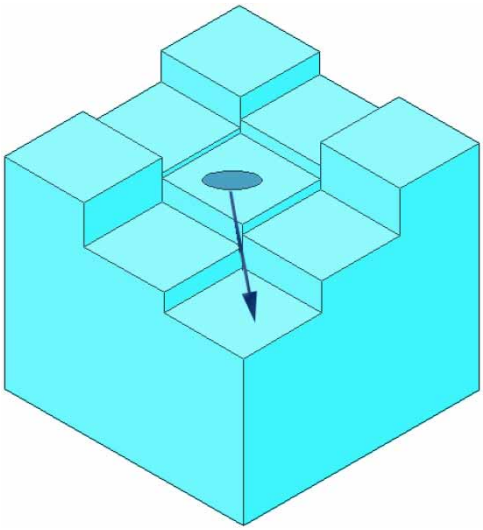

Figure 1 | Maximum gradient algorithm D8; the blue solid line is the flow direction width, the arrow is the center grid water flow, and the black solid line is the DEM grid. Please refer to the online version of this paper to see this figure in colour: http://dx.doi.org/10.2166/ws.2018.040.

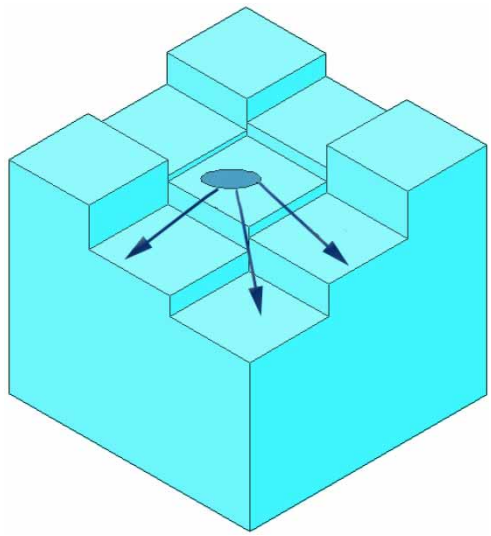

Figure 2 | Schematic diagram of the flow of the grid unit.

relatively high. It has strong data processing abilities in the concave surface of the complex watershed which includes the concave ground, depression, and flat area. Therefore, the algorithm has been widely used (Senarath *et al.* 2000; Mengelkamp *et al.* 2001). The calculation is as follows:

$$\beta_{ij} = \arctan\left(\frac{Z_i - Z_j}{D_{ij}}\right) \tag{1}$$

$$\beta_i = \max \beta_{ij} (j = 1, 2, 3, \cdots, 8) \tag{2}$$

where Z_i is the current grid cell elevation, Z_j is the height of the adjacent grid cell, D_{ij} is the distance between the centers of the two grid cells, β_{ij} is the slope of the current grid cell i pointing to the adjacent grid cell j, and β_i acts as the gradient of the real flow direction.

Quinn *et al.* (1991) proposed a multi-flow direction algorithm that is more consistent with the actual convergence situation. This multi-flow direction algorithm is in line with the actual confluence allowing a grid cell to have multiple flow directions, whereas the flow is distributed from the higher grid cells to the adjacent lower grid cells in terms of their slope ratios as shown in Figure 2. The flow distribution model adopted by the multi-flow direction algorithm is based on slope weighting (Qin *et al.* 2006), in which case the steeper downhill grid cells receive more flow. The formulas used for this algorithm are shown in Equations (3) and (4):

$$f_{ij} = \frac{S_{ij}^P}{\sum S_{ij}^P} \tag{3}$$

$$S_{ij} = \frac{Z_i - Z_j}{D_{ij}} \tag{4}$$

where f_{ij} is the flow rate assigned to the adjacent lower grid cell j by grid cell i, S_{ij} is the direction gradient from grid cell i to the grid cell j, and P is a dimensionless constant which is often 0.5.

These two algorithms, regardless of the steepest slope of the single-flow direction algorithm and the direction gradient S_{ij} in the multi-flow direction algorithm, are both types of slope determinism. This, however, ignores the role of the roughness in the grid cell flow distribution, which leads to errors in the results. Orlandini & Moretti (2009) found that the current single-flow direction algorithm included gravity as the only driving force in the distribution and aggregation process, which, it is reasonable, might cause biases. Myers (2002) established a two-dimensional mathematical laminar flow model to simulate the rough overland flow, quantify the slope flow depth, and calculate average and maximum flow rate, frictional resistance, and

other useful values. The study of the current flow allocation algorithm, however, does not consider the resistance factor of the highly estimated slope laminar flow velocity. Rueda *et al.* (2013) simplified improvements made to the D8 algorithm with respect to practicality, but the fact that the single slope factor determines the flow distribution did not change.

In the more realistic multi-flow direction, the flow of the grid cells comes from different directions to many adjacent lower grid cells. Because of the high variability of the surface features there is a difference in roughness, which affects the flow distribution in these different directions. Previous algorithms and studies have neglected the influence of this roughness on the overland runoff and flow distribution, but many studies have confirmed that these roughness factors do significantly affect slope convergence (Lane & Woolhiser 1977; Zhang & Kang 2005; Laloy & Bielders 2008; Straatsma & Baptist 2008; Luo *et al.* 2009). In addition the soil, vegetation, topography, geomorphology, hydrogeology, and other conditions are under the influence of human activities and space–time variation, and they lead to a highly fragmented patchy distribution in the watersheds. Takken & Govers (2001) believed that the changes in roughness lead to changes in runoff, soil erosion, and spatial distribution in the study area. White *et al.* (2003) used roughness as the main control parameter in overland runoff studies. The underlying watersheds that are changed on the underlying surface are reflected in the grid cells of the distributed hydrological model. Each grid unit may belong to different surface types, and even different parts of the same grid cell may consist of different types of surfaces. The high degree of crushing applied to the surfaces likely will result in different types of ground surfaces in different directions between the grid cells. These differences result in a high degree of variation in the slope roughness pace, which in turn affects the distribution of runoff in different directions. Ding *et al.* (2004) argued that the roughness coefficient of the land surface is the spatial distribution parameter, and through a series of simulations proved their argument by calculating the roughness coefficient related to the distribution of the shallow overland flow. Moreover, a method for determining the best spatial distribution of roughness coefficient also has been proposed. Sepaskhah & Shaabani (2007) found that the same ground had different roughness in the cases of different tillage and form, straight or snaking, in the process of farmland irrigation, which affected the hydraulic characteristics of the irrigation flow. Torri *et al.* (2012) studied the roughness of the slope using different particle sizes as the index, and they found that the spatial variation in the surface particle size distribution caused spatial variation in the slope roughness. Zhang *et al.* (2017a, 2017b) found that the angle between flow and vegetation rows affected the roughness coefficient in nonsubmerged conditions. The angle between flow and vegetation rows, however, had no effect on roughness coefficient under submerged conditions (Zhang *et al.* 2017a, 2017b).

Current research has not revealed the mechanism of the spatial variation of slope tillage or vegetation distribution on the overland flow. There is no consistent understanding of whether different roughness of ground flow in different directions has different values. Therefore, in this paper we used the hydraulic model test to preliminarily verify the directional difference of overland flow resistance by simulating the spatial variability of vegetation. The experimental evidence of the existence of the directional difference of flow resistance might help to improve hydrological models to simulate the flood processing on watersheds.

EXPERIMENTAL VALIDATIONS

Experiment setup

The test setup consisted of a variable slope rectangular sink, water tank, pressure gauge, and tailgate along with other components. The water tank was 5.0 m long and 0.4 m wide with a depth of 0.3 m, and the length of the test section was 3.0 m. The bottom and sidewalls of the sink were made of plexiglass. We set up two observation sections in the length of the test section and designated these as sections 1 and 2. When the observation water level was set, the distance between the two sections was 1.5 m as shown in Figure 3. We designed three plexiglass plates with different diameters of drilling, which varied by 0.003 m, to house the cylindrical rigid plants, and the cylinder height was 0.15 m. We simulated the surface conditions of the watershed with obvious band distribution and directions. Because the current grid element distributes the flow rate

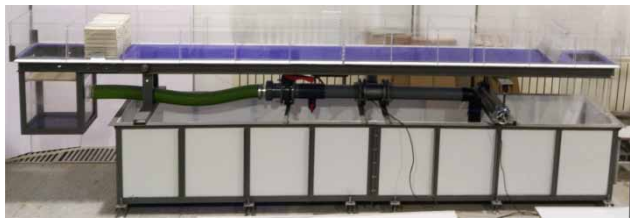

Figure 3 | Diagram of the experiment flume; the flume flow rate Q was observed by a model LDG-DN100 electromagnetic flowmeter (Hangzhou Meacon AutomationTech. Co., Ltd, Hangzhou, Zhejiang, China).

to its adjacent eight units in a distributed hydrological model, and because the angles between flow and vegetation rows were multiples of 15°, the angles between flow and vegetation rows of the cylinders in the experiment were 30°, 45°, and 90°. To make the scale mapping of the laboratory hydraulic model relatively simple, we set the distance between the adjacent cylinders of the hydraulic model test at 0.06 m. To calculate the relationship between the field crop distribution and the laboratory hydraulic model, we laid down the plexiglass plate to simulate vegetation in the tank test section. We set three slopes of 0.0%, 0.5%, and 1.0% and placed a steel pillar on the bottom of the tank to adjust the slope of the sink. A flow control valve was provided at the connection of the channel and the tank. The flow rate ranged from 0 m^3/s to 0.105 m^3/s.

Test method

We arranged the cylindrical surface of the plexiglass plate linearly in a cylindrical manner, and arranged the cylinder in the direction of the flow. In this experiment, we set up three kinds of plexiglass base plates to simulate three kinds of vegetation distributed at angles between flow and vegetation rows of 30°, 45°, and 90°, as shown in Figures 4–6. During the test, we simulated the overland flow in different directions by changing the angle between flow and vegetation rows while using the same surface conditions. The surface roughness of the watershed surface was then revealed when the overland flow went in different directions.

At each angle θ between flow and vegetation rows, we tested the three different slopes of i of 0%, 0.5%, and 1.0%, while making adjustments to the flow rate of the different flow Q test times. For each angle between flow

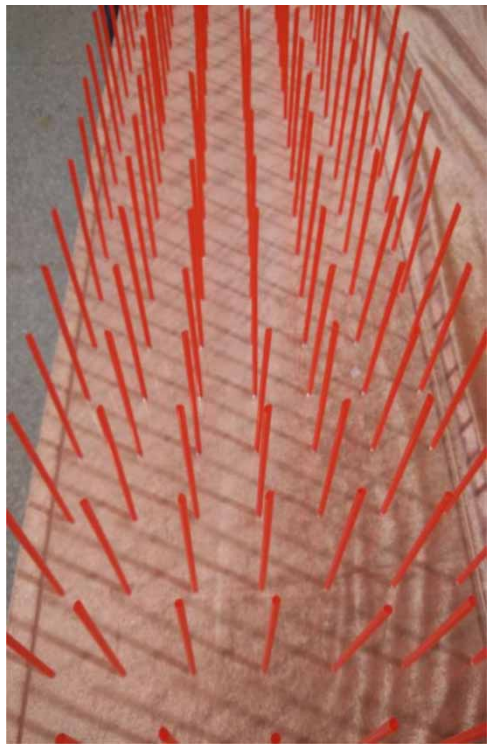

Figure 4 | A top view of the cylinder distribution at $\theta = 90°$.

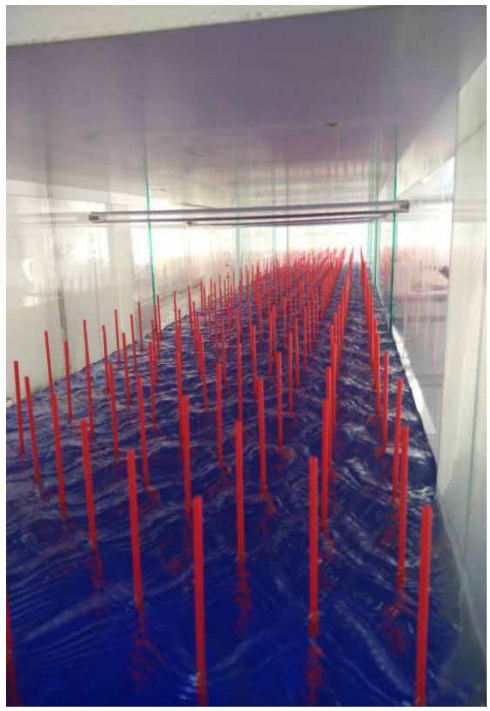

Figure 5 | Cylinder distribution front view at $\theta = 45°$.

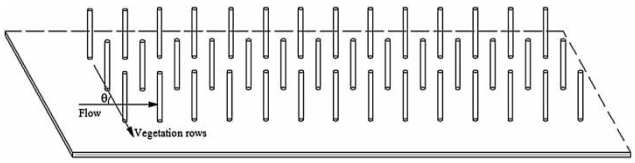

Figure 6 | Sketch of the angle between flow and vegetation rows.

and vegetation rows, the slope of ten sets of experiments, we designed three different angles between flow and vegetation rows and the three test slopes, which produced a total of 90 groups of tests conducted. We measured the pressure with the manometry tube at sections 1 and 2, and recorded the flow depth as h_1, h_2. According to the average flow depth h, flow rate Q, and other test data, we calculated v_1 and v_2 as follows:

$$v_1 = \frac{Q}{Bh_1},\ v_2 = \frac{Q}{Bh_2} \tag{5}$$

where v_1 is the flow velocity at cross section 1, v_2 is the flow velocity at cross section 2, B is the channel width, and Q is the flow rate.

In the open channel flow, the Darcy–Weisbach coefficient f, Chezy coefficient C, and Manning's roughness coefficient n are commonly used to reflect the flow characteristics of hydraulic parameters (Rouhipour *et al.* 1999; Hogarth *et al.* 2005; Smith *et al.* 2007). Among these, Manning's roughness coefficient n is considered to represent the ideal slope of overland flow parameters (Noarayanan *et al.* 2012). Therefore, we selected Manning's roughness coefficient n to characterize flow through different arrangements to the cylinders of the flow resistance. The test of the n calculation was completed as follows:

$$n = \frac{1}{v}R^{2/3}J^{1/2} \tag{6}$$

where R is the hydraulic radius, v is the average velocity of the flow between sections 1 and 2, and J is the hydraulic gradient.

We calculated the n values of the 90 sets of experiments according to Equations (1)–(6). For example, the calculation of ten sets of data at $\theta = 30^\circ$ and $i = 0\%$ is shown in Table 1.

RESULTS AND DISCUSSION

We plotted experimental data for the angles between flow and vegetation rows, flow depth, and Manning's roughness coefficient diagram, as shown in Figure 7. As shown in Figure 7(a), Manning's roughness coefficient decreases as the angle between flow and vegetation rows increases, which leads to the following relation: $n_{30^\circ} > n_{45^\circ} > n_{90^\circ}$. This relationship indicated that when the flow depth and slope were constant, the flow-blocking area of each cylinder was equivalent, and only the angle between flow and vegetation rows changed. This finding shows that Manning's roughness coefficient changes with angle between flow and vegetation rows. Figure 7(b) and 7(c) show the same changes, and thus the law of the change has no relationship

Table 1 | Experiment data and calculation results of $\theta = 30^\circ$ and $i = 0.0\%$

Trial order	Q(m³/s)	V_1(m/s)	V_2(m/s)	h_1(m)	h_2(m)	h(m)	n
1	0.00041	0.086	0.109	0.0120	0.0095	0.0108	0.0190
2	0.00102	0.115	0.134	0.0221	0.0191	0.0206	0.0243
3	0.00181	0.141	0.156	0.0320	0.0290	0.0305	0.0256
4	0.00288	0.167	0.181	0.0431	0.0398	0.0415	0.0274
5	0.00357	0.181	0.194	0.0492	0.0459	0.0476	0.0273
6	0.00427	0.190	0.204	0.0560	0.0523	0.0542	0.0295
7	0.00558	0.208	0.222	0.0670	0.0629	0.0650	0.0313
8	0.00705	0.224	0.239	0.0786	0.0736	0.0761	0.0347
9	0.00843	0.237	0.254	0.0890	0.0831	0.0861	0.0378
10	0.01057	0.258	0.275	0.1025	0.0961	0.0993	0.0386

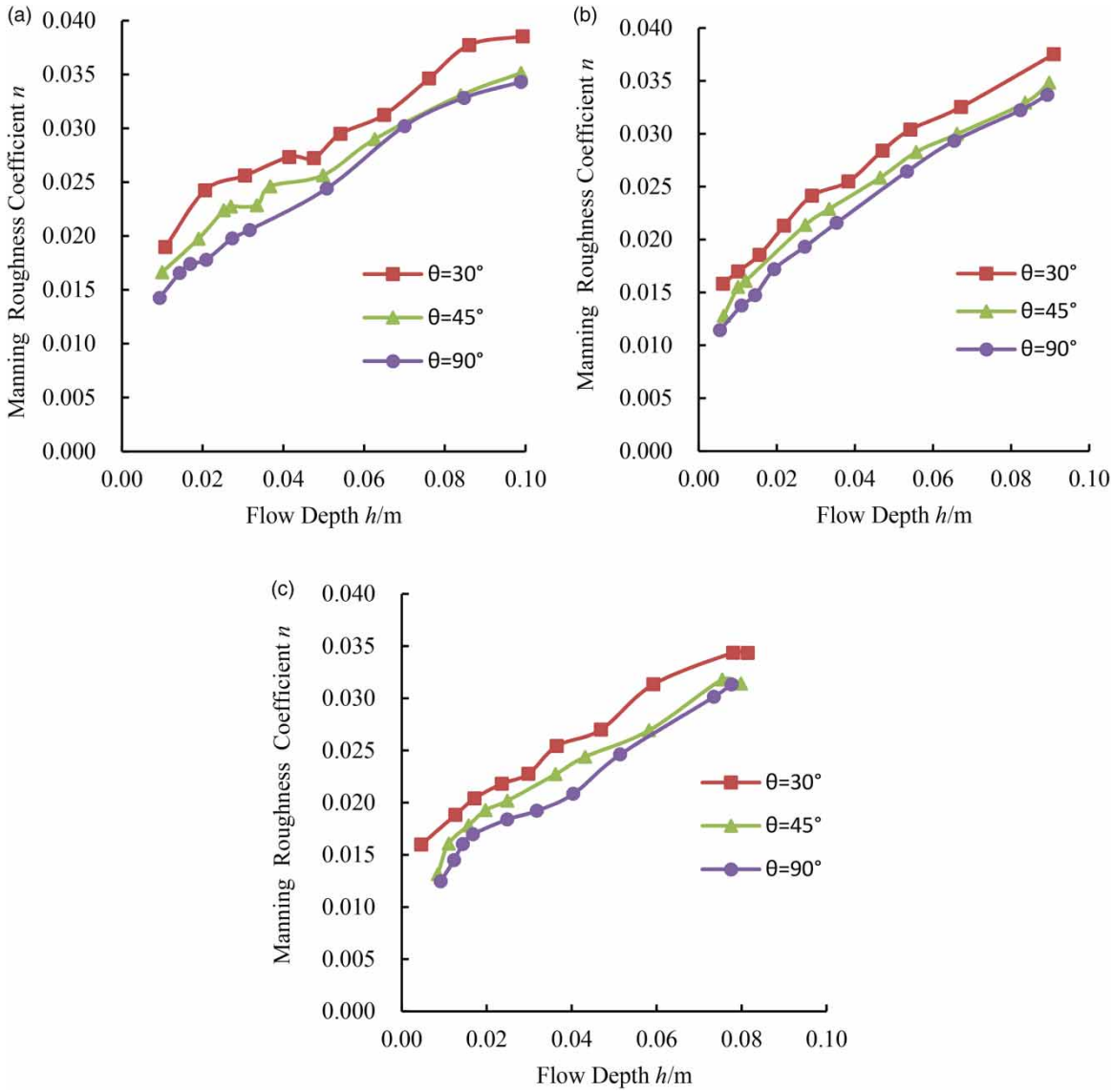

Figure 7 | The relationship of *h*–*n* under different slopes: (a) *i* is 0.0%; (b) *i* is 0.5%; and (c) *i* is 1.0%.

with slope. Further analysis showed that with the same underlying surface conditions, and flow depth, flow to different directions overland resulted in different degrees of resistance, with no respect paid to changes in the slope. When the angle between flow and vegetation rows was smaller, the vegetation resistance to overland flow was greater. This finding shows that Manning's roughness coefficient in different directions has different values. These test results align with Zhang & Kang's (2005) proposed equivalent vector roughness theory. The current multi-flow algorithm used to calculate the overland runoff direction and flow distribution, however, ignores differences in roughness overland. There was some bias with the actual condition, and if the single flow direction algorithm was used it would cause even more error.

The law of the experiment is also applicable to overland flow in modern watersheds (modern watersheds are characterized by highly complex human activities). The overland of watersheds is affected by human activities, agricultural cultivation, planting of trees and grass, and land pavement; thus, overland patches are broken. This leads the slope of the watersheds to have a vector attribute. In

the same way, different directions of the same surface will have different blocking effects on the overland flow. As the current distributed hydrological model simulates this slope convergence, we use a geographic information system to accurately separate the watershed overland into grid cells. The grid cells will converge to the adjacent downstream cells according to the DEM as shown in Figure 2. The vector attributes of the roughness of the overland will have an effect on the distribution and collection of runoff on the overland cells.

As shown in Figure 7(a), for the slope of 0.0% at the same angle between flow and vegetation rows to the vegetation conditions, Manning's roughness coefficient increases along with flow depth. This shows that the flow depth affects the value of Manning's roughness coefficient, which is consistent with the experimental results of Fraga *et al.* (2013). The area of contact between each cylinder and the flow increases along with an increase in flow depth, which implies that blocking resistance increases as flow depth increases. Therefore, flow resistance increases, and Manning's roughness coefficient increases as flow depth increases, as shown in Figure 7(b) and 7(c). It is evident that along with an increase in slope, at the same angle between flow and vegetation rows, Manning's roughness coefficient follows the same rule with an increase in flow depth. This similar result indicates that the slope does not seem to affect the law of Manning's roughness coefficient with water depth.

This analysis demonstrates that the slope does not affect the law of Manning's roughness coefficient with changes in the angle between flow and vegetation rows and flow depth. The slope will not indirectly affect the roughness overland by changing Manning's roughness coefficient by varying the angle between flow and vegetation rows and flow depth. In this study, we plotted a diagram of slope, flow depth, and Manning's roughness coefficient according to the experimental data, as seen in Figure 8. It is evident that Manning's roughness coefficient varies with the slope in the same angle between flow and vegetation rows and flow depth. Manning's roughness coefficients of different slopes show a similar range of values, thus indicating that the slope has no effect on the flow resistance. This is consistent with the experimental conclusion of Zhang (2002).

CONCLUSIONS

At present, the effect of the spatial distribution of plants is mostly neglected at the scale of single plants, which was developed by distributed hydrological models to simulate the overland flow process. Despite the spatial distribution of vegetation and the surface types, which leads to differences in overland roughness, the spatial distribution of the factor was still ignored, which contributed to significant differences between the simulation results of the distributed hydrological model and actual watershed situations (Myers 2002; Orlandini & Moretti 2009; Rueda *et al.* 2013). To study the differences of overland roughness with different directions of surface runoff confluence in watersheds, we conducted a hydraulic experiment using a variable slope test tank and cylinders. The test results revealed the following:

(1) At the same slope and flow depth, Manning's roughness coefficient decreases with an increase in the angle between flow and vegetation rows.
(2) When the slope is constant, Manning's roughness coefficient increases along with the flow depth.
(3) Under three different slopes, Manning's roughness coefficient is consistent with changes in the angle between flow and vegetation rows.
(4) Because of human activities, the surface of modern watersheds shows a distribution of plaque fragments, which leads to a vectorial attribute of overland roughness. When runoff converges, different directions of the same overland area will have different blocking effects on flow.

The aim of this experiment improved not only the current distributed hydrological process simulation, but vegetation planting and soil and water engineering practices as well, which can be used to determine the convergence flow and flow allocation of downstream grid cells. For example, when the angle between flow and vegetation rows was small, the resistive effect of vegetation on overland flow was obvious. One disadvantage of this experiment was the use of the smooth and straight plexiglass sink to simulate the natural state of the slope, which is unrealistic (i.e., for the border effect of open

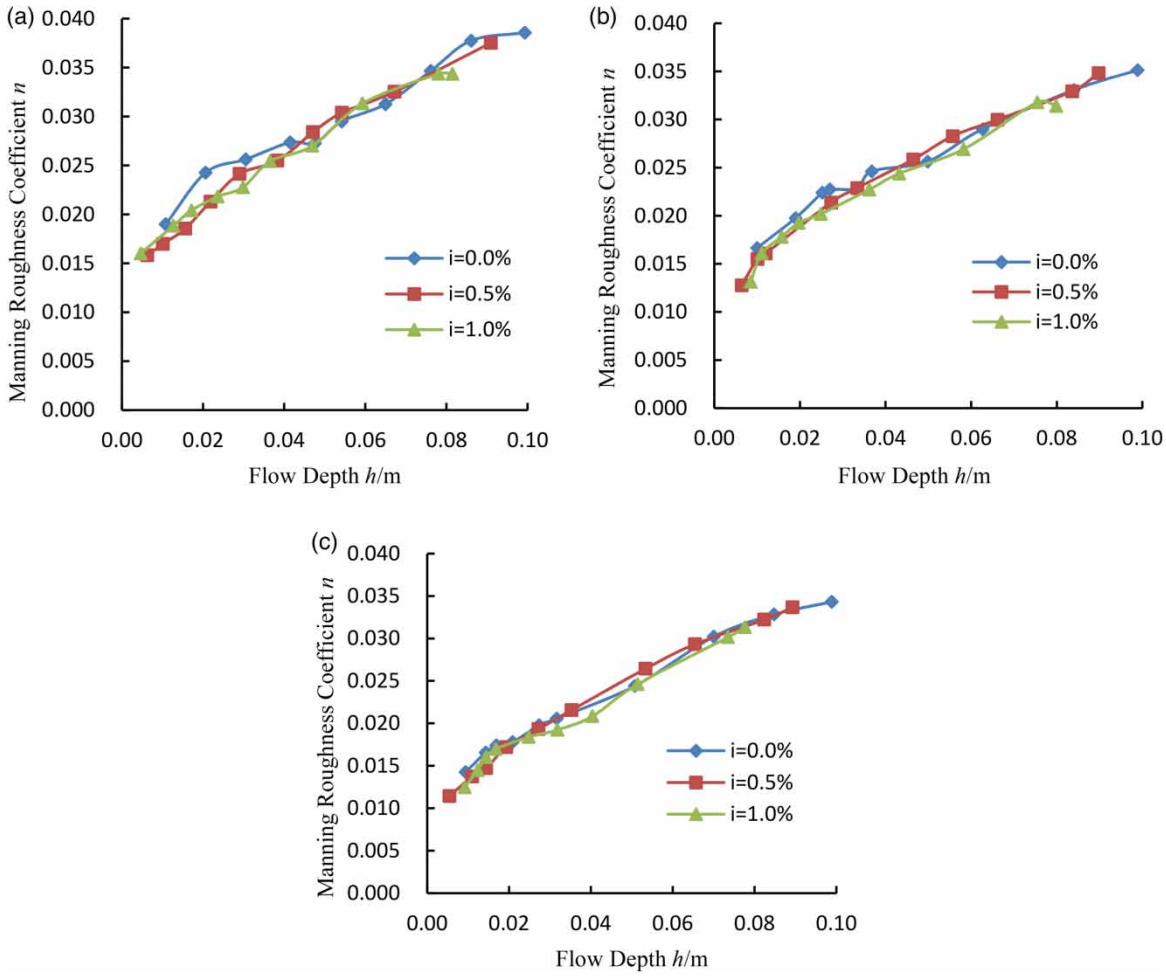

Figure 8 | The relationship of h–n under different values of angle between flow and vegetation rows: (a) θ is 30°; (b) θ is 45°; and (c) θ is 90°.

channel shapes in the experiment). Therefore, the results of this paper need to be further verified and optimized for use with respect to natural watersheds.

ACKNOWLEDGEMENTS

We would like to thank the National Natural Science Foundation of China (grant no. 41471025), the Natural Science Foundation of Shandong Province (grant no. ZR2014DM004), and the Major Research and Development Program of Shandong Province (grant nos. 2016GSF117027 and 2016GSF117036) for supporting this project.

REFERENCES

Ding, Y., Jia, Y. F. & Wang, S. S. Y. 2004 Identification of Manning's roughness coefficients in shallow water flows. *Journal of Hydraulic Engineering* **130** (6), 501–510.

Fraga, I., Cea, L. & Puertas, J. 2013 Experimental study of the water depth and rainfall intensity effects on the bed roughness coefficient used in distributed urban drainage models. *Journal of Hydrology* **505**, 266–275.

Hogarth, W. L., Parlange, J.-Y., Rose, C. W., Fuentes, C., Haverkamp, R. & Walter, M. T. 2005 Interpolation between Darcy–Weisbach and Darcy for laminar and turbulent flows. *Advances in Water Resources* **28** (10), 1028–1031.

Laloy, E. & Bielders, C. L. 2008 Plot scale continuous modelling of runoff in a maize cropping system with dynamic soil surface properties. *Journal of Hydrology* **349** (3–4), 455–469.

Lane, L. J. & Woolhiser, D. A. 1977 Simplifications of watershed geometry affecting simulation of surface runoff. *Journal of Hydrology* **35** (1–2), 173–190.

Li, Q. H. & Li, C. Z. 2000 Numerical simulation technique for routing precipitation-runoff in watershed. *Geographical Research* **19** (2), 209–216.

Luo, R. T., Zhang, G. H. & Cao, Y. 2009 Progress in the research of hydrodynamic characteristics of sediment-laden overland flow. *Progress in Geography* **28** (4), 567–574.

Mengelkamp, H.-T., Warrach, K., Ruhe, C. & Raschke, E. 2001 Simulation of runoff and stream flow on local and regional scales. *Meteorology and Atmospheric Physics* **76** (1–2), 107–117.

Myers, T. G. 2002 Modeling laminar sheet flow over rough surfaces. *Water Resources Research* **38** (11), 12.

Noarayanan, L., Murali, K. & Sundar, V. 2012 Manning's '*n*' co-efficient for flexible emergent vegetation in tandem configuration. *Journal of Hydro-Environment Research* **6** (1), 51–62.

O'Callaghan, J. F. & Mark, D. M. 1984 The extraction of drainage networks from digital elevation data. *Computer Vision, Graphics, and Image Processing* **28** (3), 323–344.

Orlandini, S. & Moretti, G. 2009 Determination of surface flow paths from gridded elevation data. *Water Resources Research* **45** (3), W03417.

Qin, C. Z., Zhu, A. X., Li, B. L., Pei, D. & Zhou, C. H. 2006 Review of multiple flow direction algorithms based on gridded digital elevation models. *Earth Science Frontiers* **3** (16), 91–98.

Quinn, P., Beven, K., Chevallier, P. & Planchon, O. 1991 The prediction of hillslope flow paths for distributed hydrological modelling using digital terrain models. *Hydrological Processes* **5** (1), 59–79.

Rouhipour, H., Rose, C. W., Yu, B. & Ghadiri, H. 1999 Roughness coefficients and velocity estimation in well-inundated sheet and rilled overland flow without strongly eroding bed forms. *Earth Surface Processes and Landforms* **24** (3), 233–245.

Rueda, A., Noguera, J. M. & Martínez-Cruz, C. 2013 A flooding algorithm for extracting drainage networks from unprocessed digital elevation models. *Computers & Geosciences* **59**, 116–123.

Senarath, S. U. S., Ogden, F. L., Downer, C. W. & Sharif, H. O. 2000 On the calibration and verification of two-dimensional distributed, Hortonian, continuous watershed models. *Water Resources Research* **36** (6), 1495–1510.

Sepaskhah, A. R. & Shaabani, M. K. 2007 Infiltration and hydraulic behaviour of an anguiform furrow in heavy texture soils of Iran. *Biosystems Engineering* **98** (2), 248–256.

Shen, X. D., Wang, L. C. & Xie, S. P. 1995 A dynamic precipitation-runoff model for a watershed based on grid data. *Acta Geographica Sinica* **50** (3), 264–271.

Smith, M. W., Cox, N. J. & Bracken, L. J. 2007 Applying flow resistance equations to overland flows. *Progress in Physical Geography* **31** (4), 363–387.

Straatsma, M. W. & Baptist, M. J. 2008 Floodplain roughness parameterization using airborne laser scanning and spectral remote sensing. *Remote Sensing of Environment* **112** (3), 1062–1080.

Takken, I., Govers, G., Jetten, V., Nachtergaele, J., Steegen, A. & Poesen, J. 2001 Effects of tillage on runoff and erosion patterns. *Soil & Tillage Research* **61** (1–2), 55–60.

Torri, D., Poesen, J., Borselli, L., Bryan, R. & Rossi, M. 2012 Spatial variation of bed roughness in eroding rills and gullies. *Catena* **90**, 76–86.

White, L. W., Vieux, B., Armand, D. & Ledimet, F. X. 2003 Estimation of optimal parameters for a surface hydrology model. *Advances in Water Resources* **26** (3), 337–348.

Zhang, G. H. 2002 Study on hydraulic properties of shallow flow. *Advances in Water Science* **13** (2), 159–165.

Zhang, S. T. & Kang, S. Z. 2005 Grid cell runoff distribution model based on vector roughness. *Journal of Hydraulic Engineering* **36** (11), 1326–1330.

Zhang, S. T., Liu, Y., Zhang, J. Z. & Liu, Y. C. 2017a Anisotropic flow resistance theory and experimental verify on partially submerged crop vegetation. *Water Science and Technology: Water Supply* **7** (1), 24–31.

Zhang, S. T., Liu, Y., Zhang, J. Z. & Liu, Y. C. 2017b Simulation study of anisotropic flow resistance of farmland vegetation. *Soil and Water Research* **12** (4), 220–228.

First received 31 August 2017; accepted in revised form 31 January 2018. Available online 15 February 2018